npj | climate and atmospheric science

Article

Published in partnership with CECCR at King Abdulaziz University

https://doi.org/10.1038/s41612-024-00838-4

Impact of fuel sulfur regulations on carbonaceous particle emission from a marine engine

Martin Bauer[1], Hendryk Czech[1,2] ✉, Lukas Anders[1], Johannes Passig[1,2], Uwe Etzien[3], Jan Bendl[2,4], Thorsten Streibel[1,2], Thomas W. Adam[2,4], Bert Buchholz[3] & Ralf Zimmermann[1,2]

Ship traffic substantially contributes to air pollution, thus affecting climate and human health. Recently introduced regulations by the International Maritime Organization (IMO) on the fuel sulfur content (FSC) caused a shift in marine fuel onsumption from heavy fuel oils (HFO) to diesel-like distillate fuels, but also to alternative hybrid fuels and the operation of sulfur scrubbers. Using multi-wavelength thermal-optical carbon analysis (MW-TOCA), our study provides emission factors (EF) of carbonaceous aerosol particles and link the fuel composition to features observed in the soot microstructure, which may be exploited in online monitoring by single-particle mass spectrometry (SPMS). Particulate matter from distillate fuels absorbs stronger light of the visible UV and near-infrared range than HFO. However, Simple Forcing Efficiency (SFE) of absorption weighted by EF of total carbon compensated the effect, leading to a net reduction by >50% when changing form HFO to distillate fuels.

Worldwide about 90% of goods are transported by ships, thereby releasing in 2011 about 0.2 million tons of fine particulate matter (PM2.5) per year in European waters[1], which has been associated with increased mortality by cardiopulmonary diseases and lung cancer[2]. Before 2020, the vast majority of ocean-going vessels were operated on heavy fuel oil (HFO), which is produced from blending the vacuum residue from crude oil refining with middle distillate. HFO is commonly defined by either a density >900 kg m^{-3} or a kinematic viscosity of >180 mm^2 s^{-1} at 15 °C. The oil consists of high-molecular weight hydrocarbon structures and contains sulfur in the range of few percent by mass[3] as well as substantial amounts of transition metals, such as vanadium, nickel and iron, which are emitted in the PM2.5 fraction[4]. In contrast to diesel cars and trucks, ships are usually not equipped with aftertreatment devices common in road traffic, such as particle filters or oxidation catalysts. Moreover, the upper limits for the fuel sulfur content (FSC) for ships are orders of magnitude higher compared to road traffic, hence ships exhibit high emission per mass of consumed fuel or generated amount of energy especially for SO_x and PM2.5[5,6]. Furthermore, ships typically have either one large slow-speed two-stroke engine and several auxiliary medium-speed four-stroke engines, or several four-stroke engines for propulsion and power generation with different emission patterns[7].

In order to reduce the environmental burden of maritime traffic, the International Maritime organization (IMO) introduced a global FSC cap of 0.5% beginning in 2020. In addition to that measure, previously defined Sulfur Emission Control Areas (SECA) have been introduced, where only fuels with a maximum FSC of 0.1% are allowed[8]. Furthermore, a new measure starting in July 2024 set an upper limit for fuel viscosity in the Arctic[9]. The sulfur cap *de facto* prohibited the use of most HFO and led to a shift in the marine fuel market towards distillate fuels, such as marine gas oil (MGO), and hybrid fuels containing minor amounts of high-molecular weight hydrocarbons above the boiling point range of middle distillate[10]. Alternatively, ships may be still operated on HFO, but only combined with sulfur scrubbing aftertreatment technology, titrating SO_x with sea water (in open-loop mode) or an alkaline solution (in closed-loop mode)[11,12].

Modeling and epidemiological studies have quantified significant public health benefits from the switch to low-sulfur fuels in terms of reductions in air pollutants, such as PM2.5, sulfate, metals and SO_x[13,14]. As a drawback, increased NO_x values have been observed in the North and Baltic Sea[15]. Furthermore, a substitution of HFO by diesel-like fuel reduces acute toxicity in human lung epithelial cells[16], but PM2.5 from diesel fuel combustion affected several essential pathways of lung cell metabolism even stronger[17].

Beyond public health, ship emissions directly or indirectly affect the climate. Direct effects include the release of greenhouse gases, such as carbon dioxide, methane and nitrous oxide, and modification of the Earth's

[1]Chair of Analytical Chemistry, Institute of Chemistry, University Rostock, 18059 Rostock, Germany. [2]Cooperation Group "Comprehensive Molecular Analytics", Helmholtz Centre Munich, 85764 Neuherberg, Germany. [3]Chair of Piston Machines and Internal Combustion Engines (LKV), Faculty of Mechanical Engineering and Marine Technology, University of Rostock, 18059 Rostock, Germany. [4]Institute of Chemistry and Environmental Engineering, University of the Bundeswehr Munich, 85579 Neubiberg, Germany. ✉e-mail: hendryk.czech@uni-rostock.de

radiative forcing by PM2.5 components, predominantly black carbon (BC) but also brown carbon (BrC) including tar[18,19]. Indirect effects comprise the ability of PM2.5 to initiate cloud formation, which increases the albedo of the atmosphere, associated with a cooling effect[20]. Lower FSC leads to lower emissions of hygroscopic sulfate particles but higher fraction of hydrophobic soot particles, which reduces the cloud formation ability of the emissions and thus the cooling effect. Therefore, benefits for public health achieved by regulating the FSC are associated with increasing radiative forcing[21].

Our study examines different emission scenarios from a marine four-stroke engine operated on non-compliant fuels (representing emissions before 2020), globally compliant fuels as well as fuels compliant with current FSC limits in SECA (Supplementary Table S1). Despite its comparably low power of 80 kW, the engine was shown to produce emission representative for larger ocean-going vessels[22]. Filter samples of PM2.5 were measured by a multi-wavelength thermal-optical carbon analyzer, combining established carbonaceous aerosol quantities of organic carbon (OC) and elemental carbon (EC) with their optical properties[23] for comparing emission factors (EF) and changes in physical-chemical properties of the particulate emissions. Finally, distinct differences in the structure of EC is exploited in single-particle mass spectrometry (SPMS) as an extension of recent progress in remote online identification of marine fuels from ship plume analysis based on ultrasensitive detection of transition metals[24] and the pattern of polycyclic aromatic hydrocarbons (PAH)[25].

Results

Emission factors of OC and EC

Emission factors of OC and EC from individual engine loads (Supplementary Table S2) were calculated as weighted averages according to the IMO engine test cycle E2 for six marine fuels: hydro-treated vegetable oil (HVO), marine gas oil (MGO), ultra-low-sulfur aromatic rich heavy fuel oil (ULS-HFO$_{ar}$), low-sulfur heavy fuel oil (LS-HFO), synthetic high-sulfur heavy fuel oil (HS-HFO$_{syn}$), and high-sulfur heavy fuel oil (HS-HFO) (Fig. 1). HFO with high FSC (HS-HFO and HS-HFO$_{syn}$), which were widely used before 2020, led to emission factors for OC and EC in the order of 200 to 500 mg kWh^{-1}, agreeing with previous studies on research engines and ongoing vessels[12,26,27]. Compliant LS-HFO did not show any significant emission reduction for neither OC nor EC compared to HS-HFO$_{syn}$ or HS-HFO. Therefore, the chemical composition of the used HFO is the driving force for carbonaceous particulate emissions, while the FSC alone had no substantial effect.

In SECA, most ships are operated on distillate fuels such as MGO[28], which has been shown to produce significantly lower emissions of both OC and EC than heavy fuels in our study, while the ratio of OC to EC remains around unity. Since only the FSC is regulated, SECA-compliant fuels can also be obtained from alternative production methods. ULS-HFO$_{ar}$ originates from a cycle oil, a side product of the crude oil refining, which is rich in two- to four-ring aromatic hydrocarbons but low in sulfur due to hydrocracking of heavy crude oil fractions. Operating the engine on this hybrid fuel, with properties in between conventional HFO and MGO, has implications for the toxicological properties of the emissions due to its high content of PAH[29], but does not significantly increase emissions of OC and EC compared to MGO. In view of potentially carbon-neutral fuels, hydro-treated vegetable oil (HVO) inherently having a low FSC may be used in the future as an alternative fuel in SECA. Carbonaceous emissions from engine operation on HVO did not drop below emissions from MGO engine operation, so additional costs for fuel did not lead to a reduction in PM emissions. However, engine conditions in this study were optimized for operation of HFO, thus optimized operation of HVO may still lead to a reduction of unexpectedly high OC and EC emissions in this study.

The individual engine loads cause different EF for both OC and EC (Supplementary Table S2). In all HFO-labeled fuels, the average EF of carbonaceous emissions consistently decreased as engine loads increased, whereas this trend was less apparent for distillate fuels. Generally, limitation of the FSC to 0.5% had small effects on the carbonaceous emissions if conventional HFO of proper fuel quality is used (LS-HFO and HS-HFO). The observed reduction in emissions related to the IMO engine test cycle E2 (Fig. 1) by switching from heavy to distillate fuels are mainly caused by lower emissions at 25% engine load.

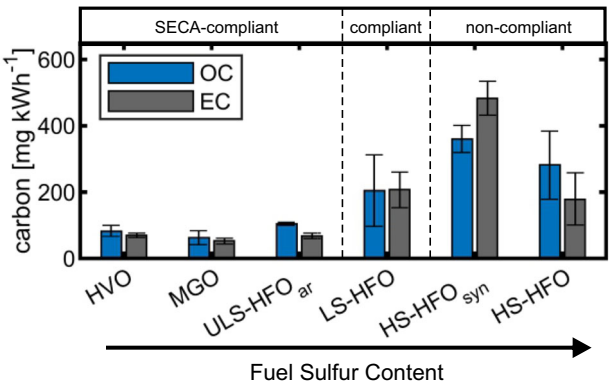

Fig. 1 | Emission factor of OC and EC. Emission factors of organic and elemental carbon (OC, EC), weighted according IMO engine test cycle E2, for marine fuels of different fuel sulfur compliance levels. Error bars denote the standard deviation from $n = 5$.

Composition of carbonaceous aerosol particles

Thermal-optical carbon analysis (TOCA) allows speciation of carbonaceous aerosol particles according to thermal fractions in the temperature protocol *ImproveA*, defining four fractions of OC (OC1-OC4) and three fractions of EC (EC1-EC3) as well as pyrolytic OC (OC$_{pyro}$) from the optical correction of charring. In this study, the approach by Han et al. (2007)[30] is used, dividing EC into char-EC (referring to EC1) and soot-EC (referring to the sum of EC2 and EC3), which accounts for differences in thermal refractiveness and consequently in soot microstructure.

For most carbonaceous emissions, the relative OC content of the total carbonaceous emissions occurred in a moderately small range of 0.425 to 0.75 regardless the fuel (Fig. 2), which is equivalent to ratios of OC to EC (OC/EC) from 3 to 0.74. The majority of all individual sample measurements appeared in the OC content range of 0.36 to 0.8 equivalent to OC/EC from 4 to 0.56 (Supplementary Fig. S1). At higher engine loads, the share of fractions OC1 and OC2 with the lowest thermal refractiveness decreased, while OC fractions of higher thermal refractiveness increased towards higher loads, but trends for fuels can be identified (Supplementary Fig. S2). However, a higher contribution of soot-EC is striking for the diesel-like fuels MGO and HVO, whereas a higher percentage of char-EC can be observed for conventional HFO usage. This also holds for HS-HFO and HS-HFO$_{syn}$ emissions after exhaust gas treatment by an open-loop sulfur scrubber, which enables cruising with FSC larger than 0.5% outside SECA[11]. The aromatic-rich but low-viscous HFO (ULS-HFO$_{ar}$) belongs to the group of so-called "hybrid fuels". It features both properties of distillate fuel and conventional HFO and also the ratio of char-EC to soot-EC appear between those fuel classes with approximately 0.5 (Fig. 2).

Connecting the operationally defined quantities char- and soot-EC from TOCA[30] with the re-classification of light-absorbing carbon by Corbin et al.[19] and fuel properties (Supplementary Table S1), the observations may be explained as following. HFO refers to a dense, highly viscous and low-volatile fuel, which may have a kinematic viscosity of up to 380 mm^2 s^{-1} at 50 °C and a density of up to 0.990 g cm^{-3} at 15 °C, compared to 2 mm^2 s^{-1} and 0.835 g cm^{-3} for MGO in this study (Supplementary Table S1). Hence, during fuel injection, droplets do not fully vaporize and cause locally fuel-rich mixtures, thus surface graphitization occurs by fuel droplet pyrolysis[19,31]. Droplets from spray injection of diesel-like fuels quickly evaporate, so hydrocarbons of the diesel-like fuels thermally decompose into radicals and form soot particles. Hence, engine operation with HVO and MGO generates soot structures different from HFO engine operation.

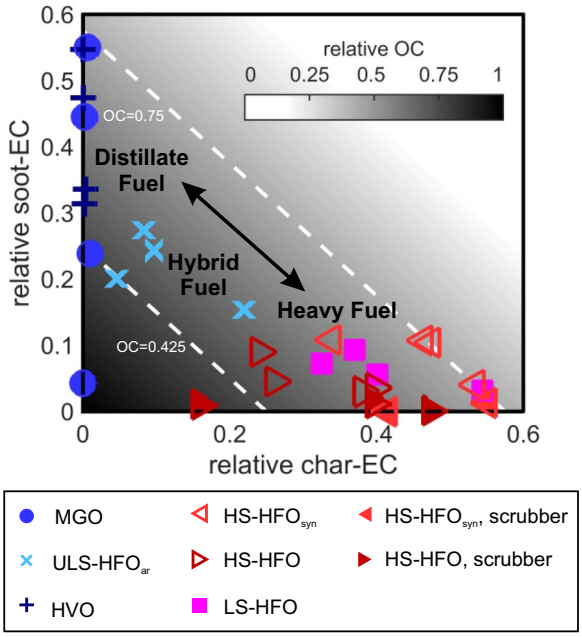

Fig. 2 | Distributions of OC, char-EC and soot-EC. Fractions of OC, char-EC (EC1) and soot-EC (EC2 + EC3) of all 24 fuel/engine load combinations. Two branches of the diesel-like fuels HVO and MGO with low char to EC ratio on the one hand and LS-HFO, HS-HFO$_{syn}$ and HS-HFO with high char to EC on the other are apparent, with ULS-HFO$_{ar}$ in between. Dashed lines denote the space of relative OC from 42.5 to 75% where 90% of the experiments fall in. Filled red triangles refer to HS-HFO$_{syn}$ and HS-HFO emissions after open-loop wet scrubber from Jeong et al.[11].

In TOCA during *ImproveA* temperature protocol, graphite layers of char-EC are immediately oxidized along with pyrolytic OC when oxygen is added to the helium atmosphere due to the porous structure and thus larger surface area[32]. Moreover, tar from partial pyrolysis of fuel droplets may also account for EC1, especially in engine operation with HFO, and contains a lower degree of graphitization than in char[19]. In contrast, soot-EC originates from radical reactions in the flame (flame synthesis), building up graphitized soot from hydrocarbon radicals via soot inception. Those soot particles are smaller and more compact, thus less prone to oxidation[32] and quantified at higher temperatures in EC2 and EC3 during TOCA with *ImproveA*.

ULS-HFO$_{ar}$ refer to a SECA-compliant HFO with high aromatic content, but a density similar to conventional HFO and a viscosity as low as diesel-like fuels. In agreement with that, emissions of EC were comprised of comparable char- and soot-EC content. On the one hand, the low viscosity of ULS-HFO$_{ar}$ compared to conventional HFO generates smaller and faster evaporating fuel droplets after injection. It improves the decomposition of the fuel into small hydrocarbon radicals, leading to soot formation by flame synthesis instead of char formation by droplet pyrolysis. Moreover, the small aromatic hydrocarbons in the fuel are intermediate products during flame synthesis and enhance the soot particle formation further. On the other hand, the high fuel density may cause locally fuel-rich zones through slower droplet vaporization, as indicated by the poor ignition ability and limited use at higher engine load of the ULS-HFO$_{ar}$[11], generating char particles by pyrolysis. Based on the obtained result of EC, both processes appear at comparable importance.

An alternative explanation for the observed abundancies of char- and soot-EC may be the content of metals and sulfur, which inversely correlates with the detection of soot-EC except for HS-HFO$_{syn}$ (Supplementary Fig. S3). Metals and oxygen-containing anions, such as sulfate, are known to promote EC oxidation in thermal analysis[33] but also suppress the formation of soot and soot precursors already during the combustion[34,35]. When ships change their fuels at crossing the border into a SECA, it requires time until the fuel has been completely exchanged in all parts of the fuel system and injection pumps, including metal-containing residues of previously used heavy fuels. Khan et al.[36] reported 84 and 90 min until SO_2 emission concentrations have decreased by 95% after changing from HFO to MGO for an ocean-going vessel. However, the metal content between HFO and MGO differs by two orders of magnitude, hence even a longer switching time would be necessary for metal concentrations approaching those of MGO, assuming that metals exhibit the same behavior as sulfur. As the metal content of the particulate emissions depends on the fuel metal content, fuel switching times likely shift the distribution of evolving carbon to less refractive carbon fractions[37].

In addition to shifts in EC oxidation, the water content of the filter samples as well as the high load of organics proved challenging for the exact determination of EC in PM emissions of ships, affecting the split between OC and EC[37,38]. However, the detected amount of pyrolytic OC was low compared to EC1, hence the ratio of soot-to-char EC cannot be significantly smaller.

EC in slow-speed two-stroke engine emissions are dominated by char-EC regardless of the fuel, while only medium-speed four-stroke engines operated on distillate fuel reveal significant contributions by soot-EC[27,39,40], which agrees with the findings of this study. Hence, the EC fractions may provide an additional fuel-sensitive indicator for ship emissions from auxiliary engines regardless of sulfur scrubber operation. However, at the borders of SECA when fuel switching is required, residues of bunker fuel might affect the EC classification of the emission although distillate fuel is used.

Optical aerosol properties

For allocating absorption of PM2.5 (represented by TC) from the marine engine into BC and BrC, an Angström Absorption Exponent (AAE) of unity and that absorption by BC only happens in the near infrared (NIR) was assumed. For HFO, BrC-related absorption (>5% of total absorption at 405 nm and 450 nm) was only detected at 25% engine load, which is in agreement with previous studies[18,19] and illustrated by AAE larger than unity with the exception of HVO (Fig. 3 top). However, the observed contribution to light absorption by BrC in MGO emissions at 25% engine load, as indicated by an AAE of 1.6, was likely caused by no measurable content of EC. Largest contributions of BrC to total absorption at 405 and 450 nm were found for ULS-HFO$_{ar}$ and HS-HFO with 30% and 15%, respectively. Nevertheless, the majority of absorption in the spectral range from 405 to 980 nm could be explained by BC for all fuels.

Owing to the differences in soot structure, engine operation on diesel-like fuels HVO and MGO generates stronger absorbing particles, indicated by the mass absorption efficiency (MAE$_{TC}(\lambda)$) integrated over wavelengths from 405 to 980 nm (Fig. 3 top). The MAE$_{TC,\lambda}$ of the seven individual wavelengths of the MW-TOCA may be found in Supplementary Table S3. Interestingly, ULS-HFO$_{ar}$ revealed the largest AAE among all fuels, but comparably low MAE$_{TC,\lambda}$. Overall, marine fuels compliant with the global sulfur limit may have manifold effects on light-absorbing properties of ship particulate emissions, driven by various physical and chemical fuel properties.

The Simple Forcing Efficiency (SFE) was introduced by Chen & Bond (2010)[41] to obtain the quantitative radiative effect of aerosol particles per mass in [W g^{-1}]. Here, a reduced approached of SFE is used without the effect of aerosol particles on scattering and integrated from 405 to 980 nm according to:

$$SFE_{405}^{980} = \tau_{atm}^2 \times (1 - F_c) \times a_s \times \int_{405nm}^{980nm} MAE_{TC}(\lambda) \times \frac{S(\lambda)}{4} d\lambda \quad (1)$$

where S(λ) is the solar radiation spectrum at 37° angle of incidence (AM15G) in W m^{-2} in steps of 1 nm, τ_{atm} is the atmospheric transmission, F_c is the cloud fraction, and a_s is the surface albedo. The same atmospheric scenario for τ_{atm}, F_c, and a_s was used as in Tian et al. [42], which denotes global averages of 0.79, 0.6 and 0.19, respectively. Other climate scenarios can be

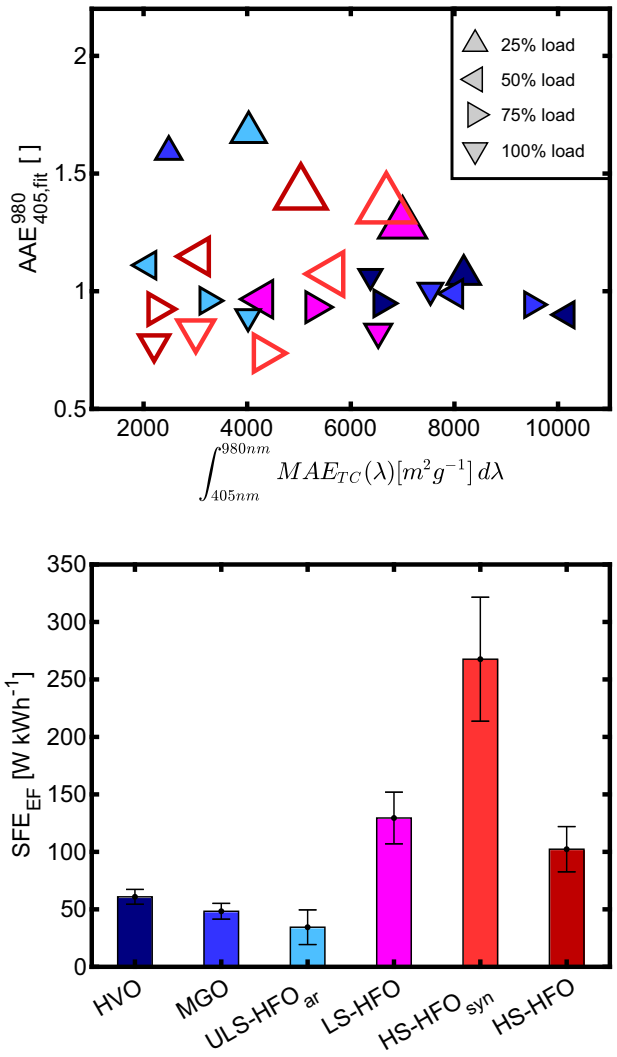

Fig. 3 | Absorption weighted by EF_{TC}. Top: Angström Absorption Exponent (AAE) from exponential fit vs. the integrated mass absorption efficiencies related to total carbon (MAE_{TC}) from 405 to 980 nm for individual engine loads. Marker sizes increase with emission factor of total carbon (EF_{TC}). Open symbol indicates non-compliant fuels with colors as labeled below. Bottom: Sime Forcing Efficiency Emission Factor (SFE_{EF}) integrated from 405 to 980 nm and weighted according to the IMO cycle E2. Errorbars were derived from the integrated 95% confidence prediction band from λ vs. $MAE_{TC}(\lambda)\times EF_{TC}$ (Supplementary Fig. S4).

easily adapted to change quantitative SFE, however, the consequences of fuel switching remain unaffected in this approach.

In order to take quantitative emission data for light-absorption into account, $MAE_{TC}(\lambda)$ in m^2 g^{-1}, obtained from a power law fit of λ vs $MAE_{TC}(\lambda)$ (Supplementary Fig. S4), were multiplied with EF_{TC} in g kWh^{-1} and weighted according to the IMO cycle E2.

$$SFE_{EF} = SFE^{980}_{405} \times EF_{TC} \quad (2)$$

The SFE_{EF} shows a similar pattern (Fig. 3 bottom) to the emission factors for OC and EC (Fig. 1). Switching from the three HFO to SECA-compliant fuels reduced the SFE_{EF} by a factor of two to seven, depending on the individual considered fuel. Particularly engine operation on low-grade HFO, such as HS-HFO_{syn} of this study, generates the most intense light absorption in the spectral range from 405 to 980 nm per kWh of produced energy. LS-HFO and HS-HFO comprising of compounds with a smoother volatility continuum show similar SFE_{EF} despite a difference in FSC of 1.7 percentage points.

Although ULS-HFO_{ar} as a hybrid fuel appeared in between typical HFO and diesel-like fuels, it features the lowest SFE_{EF}. Similar to typical HFO, the $MAE_{TC,\lambda}$ for ULS-HFO_{ar} was lower than for MGO and HVO, but emission factors appeared closer to the diesel-like fuels. Therefore, considering light absorption of its carbonaceous material, ULS-HFO_{ar} has the lowest immediate climate effects among the six studied fuels. However, other criteria including direct climate effects by light scattering, indirect climate effects by induced cloud formation[20], and possibly more health-relevant emissions through the enhanced release of PAH and sustainable engine operation must be considered for an evaluation of the benefit from lower SFE_{EF}.

Identification of marine fuel operation by elemental carbon analysis

Based on EC fractions in the *ImproveA protocol*, fuel classes of HFO, diesel-like fuels and hybrid fuels may be distinguished in the laboratory. Due to the distinct effect of the fuel properties on the nature of EC, it was hypothesized that the EC structure of those particles is reflected in the distribution of carbon clusters produced by laser desorption/ionization in single-particle mass spectrometry (SPMS). This information may increase the confidence in the identification of ship particulate emissions based on traces of transition metals[24] and the molecular signatures of PAH using resonance-enhanced multiphoton ionization (REMPI)[43,44], providing ship fuel identification in real-time. In fact, the clustering algorithm applied to 5000 LDI anion mass spectra of carbon fragment ions $^{12}C_n^-$ for $n = 2, 3, \ldots, 9$ for compliant fuels MGO, LS-HFO and ULS-HFO_{ar} at 75% engine load generated 7 distinct cluster centers, which were dominated by one of the three fuels (Fig. 4). Dependent on the fuel, the pattern of the cluster centers show the highest relative contribution of small ($1 < n < 4$), medium ($3 < n < 7$) and large ($6 < n < 10$) $^{12}C_n^-$ for LS-HFO, MGO and ULS-HFO_{ar}, respectively. Char particles, which are mainly associated with conventional HFO emissions, might decompose to smaller carbon fragment ions on a larger scale because of their porous morphology compared to the more compact soot particles, which are mainly associated with MGO emissions (Fig. 4). Specifically, clusters with highest contribution by ULS-HFO_{ar} particles contained large ($6 < n < 10$) C_n^-, which might be a result of higher initial availability of soot particle precursors and consequently more intense soot inception, but these clusters contribute less to the total cluster weights. However, a larger dataset and complementary measurements of ongoing ships are necessary to confirm the findings and to demonstrate the applicability for remote fuel identification from mid-range transport of ship plumes.

Discussion

Regulations of the FSC by the IMO in the past decade led to an overall shift of marine fuels from HFO, or generally called bunker fuels, to distillate fuels with an intrinsically lower FSC, such as MGO[10]. However, due to the higher price of distillate fuels, other solutions for ship owners became attractive, including low-sulfur bunker fuels, hybrid fuels with properties between typical HFO and MGO but compliant with FSC limits, and the installation of sulfur scrubbers, still enabling engine operation with high-sulfur bunker fuels. Sulfur scrubbers are an investment, which have to redeem for the ship owner, hence sulfur scrubbers are most attractive if the price spread between MGO and HFO is large and especially for ships of a higher lifespan[45]. For older ships, low-sulfur fuels are economically more favorable, but they span a broad range of chemical composition due to its different manufacturing process[3], which complicates an assessment of possible benefits and drawbacks from FSC regulations on public health and climate. Furthermore, it requires a reassessment and further development of markers for the detection of ship emission in the atmospheric environment.

Regarding carbonaceous emissions, our study demonstrates that the FSC is not the determining factor. LS-HFO and HS-HFO of similar quality had comparable EF, whereas the HS-HFO_{syn} with discontinuous boiling behavior caused significantly higher EF for both OC and EC. Therefore, the global sulfur cap to FSC of 0.5% does not seem to affect OC and EC emissions if heavy fuels are still used, but ULS fuels with an FSC < 0.1% lead

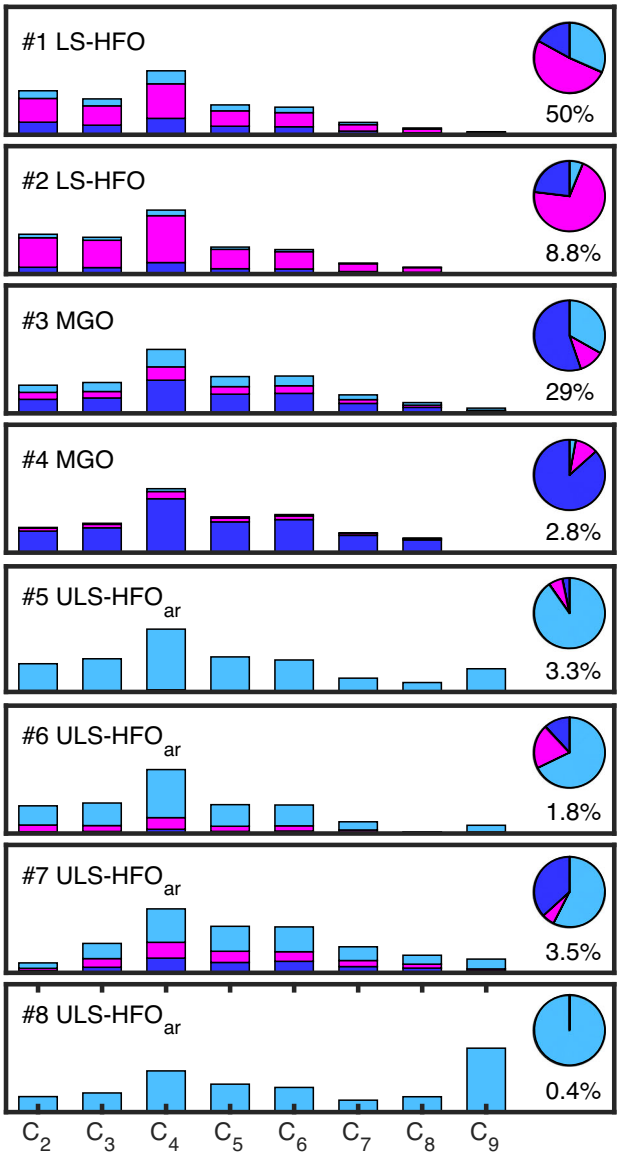

Fig. 4 | Eight clusters of typical C_n distributions in the mass spectra of anions from 5000 single particles for each of the three fuels. Cluster names are derived from the fuel that contributes most to the cluster. The particle number contributions of the fuels are shown as pie charts while the signal contribution is color-coded. Percentages denote the contribution of the individual cluster to the total number of detected particles. Apparently, the bunker fuel LS-HFO with a dominant char content produces smaller carbon fragments while the soot-dominated particles from distillate fuels lead to larger carbon fragments with the ULS-HFO$_{ar}$ in between. (0.5% FSC compliant fuel: LS-HFO (magenta) and SECA compliant fuels: MGO (dark blue) and ULS-HFO$_{ar}$ (light blue)).

to a significant reduction in EF for both OC and EC by a factor of 2–2.5 compared to LS-HFO and HS-HFO, regardless their differences in chemical fuel composition. Therefore, the introduction of SECA has basically a benefit for public health by lower OC and EC emissions, assuming equal toxicity of PM2.5 from all fuels. However, a recent study exposing human lung cells to PM2.5 from marine fuels demonstrates that this is not a justified assumption[29] and may be used to refine health benefits from FSC regulation.

Only an upper FSC limit of 0.1% as currently applicable in SECA shows a decrease in OC and EC emissions because it shrinks the range of compliant bunker fuels to an extend that lighter fuels with lower EF prevail. However, even in SECA this may be circumvented by using sulfur scrubbers, which do not significantly affect the quantitative emissions of PM2.5 but EC or equivalent BC[11] and the composition of high-molecular weight compounds[46].

For the Arctic, new measures become into force in July 2024, prohibiting fuels with a kinematic viscosity larger than 180 mm^2 s^{-1}, and thus banning engine operation on conventional HFO. However, emerging hybrid fuels, such as ULS-HFO$_{ar}$, are not covered by this legislation. Considering that unburned fuel is a major contributor to organic ship emissions[47], the combustion of ULS-HFO$_{ar}$ releases large amounts of two- to four-ring PAH, which are potent precursors of secondary organic aerosol (SOA). Therefore, to reduce secondary PM2.5 from ships and especially to protect sensitive environments such as the Arctic region, a more precise regulation would be required.

Among all three SECA-compliant fuels, the EF of TC were not significantly different despite their distinct difference in origin and chemical composition as well as in market price. Moreover, considering the EF and absorption properties of the carbonaceous emissions in SFE$_{EF}$, a similar ranking of the fuels is obtained as for EF. Therefore, from an economic perspective and for the effect on direct radiative forcing, ULS-HFO$_{ar}$ has the lowest cost/benefit ratio when disregarding its unfavorable ignition behavior and incapability for operation at full engine load. However, particularly PAH-derived health effects and enhanced SOA formation from intermediate-volatile PAH may cancel out low costs and low SFE$_{EF}$. Without considering direct light scattering and indirect effects with a negative effect on radiative forcing, differences between the SFE$_{EF}$ of ULS fuels and LS-/HS-HFO is supposedly smaller. Overall, since 2020 there is evidence for microphysical changes of clouds, also driven by the release and formation of primary and secondary sulfate, and increased radiative warming caused by fuel sulfur legislation on FSC[48,49].

In order to identify marine fuels for operation in ocean-going vessels, SPMS has been shown to provide relevant information from online ship plume measurements in real-time. In addition to the traditional markers vanadium and nickel together with sulfur-related ions[50], the evaluation of polycyclic aromatic compounds[51], and the ultra-sensitive detection of metals by resonant ionization[52] have been developed and used for ship emission studies. This distribution of char- and soot-EC from MW-TOCA is resembled in the pattern of carbon clusters in negative LDI ions where char-EC tends to generate slightly smaller C_n ions than soot-EC. However, the aromatic-rich fuel ULS-HFO$_{ar}$ had distinct contributions from larger C_n, possibly owing to a different soot microstructure than from predominantly aliphatic fuels, such as observed for benzene and n-hexane combustion in diffusion flames[53]. Combining the abundance of sulfur species, PAH pattern, and signature of transition metals with carbon clusters, SPMS is able to identify marine fuels from plume measurements in greater detail, offering a technology for monitoring fuel compliance concerning FSC and potentially beyond.

The main limitation of the findings of this study are their restriction to a four-stroke marine engine, which are typically either used as main engines of smaller ships or as auxiliary engines on larger ones. Main engines of large cargo vessels or tanker are two-stroke engines with different operation principles, fuel requirements and emission pattern. Therefore, further research on two-stroke engine is required to understand indirect effects for climate and public health from latest IMO regulations on FSC and fuel viscosity in the Arctic.

Similar to other transportation sectors, marine traffic is heading for decarbonization or shifts to carbon-neutral fuels from biogenic feedstock, recycling or reusing[7]. Particularly those which are carbon-free, including hydrogen and ammonia, or burned together with a carbon-based pilot fuel necessary for improved ignition, will change the physical-chemical properties of particulate emissions and consequently bring up new challenges for source identification of marine combustion engines and consequences for climate and health.

Methods

Engine operation, marine fuels and PM2.5 sampling

Particulate emissions were investigated from a direct injection four-stroke, single-cylinder research marine engine of 80 kW nominal power, which was operated at four individual loads (25, 50, 75 and 100%) and six marine fuels with different levels of sulfur compliance. Five independent repetitions were

conducted for each combination of engine load and fuel, so 120 samples were collected in total.

High-sulfur heavy fuel oils (HS-HFO and HS-HFO$_{syn}$) exceed the maximum FSC of 0.5% and are therefore not compliant anymore since 2020 without exhaust aftertreatment. The subscript "syn" indicates that this fuel was produced by artificial blending of vacuum distillation residue with middle distillate fuel, in order to generate a boiling gap and thus a low-grade fuel; HS-HFO denotes a commercial marine bunker fuel. LS-HFO also refers to a commercial HFO, but with a FSC of 0.5%, so it can be used outside SECA. Inside SECA, marine gas oil (MGO) is a commercial compliant fuel, which has high similarity to diesel and a FSC of 10 ppm. Furthermore, hydrotreated vegetable oil (HVO, FSC < 10 ppm) and ultralow-sulfur aromatic-rich heavy fuel oil (ULS-HFO$_{ar}$, FSC of 0.06%) were tested as alternative SECA-compliant fuels. HVO is obtained from the hydrogenation of vegetable oil. It is chemically composed of alkanes, lighter than MGO and has an intrinsically lower level of impurities including heteroatoms and metals, hence regarded as "clean" fuel. Since the engine was operated with optimized settings for bunker fuels, there is still potential to lower emissions from HVO combustion. Despite being classified as HFO due to its high density, ULS-HFO$_{ar}$ is highly similar to distillate fuels like MGO in terms of sulfur, metal content, viscosity, and flash point. This cycle oil is produced from the fluid catalytic cracking of crude oil and predominantly composed of alkylated 2- to 4-ring aromatics. As expected from the high calculated carbon aromaticity index (CCAI) of 907, slightly exceeding the common range from 800 to 880, ULS-HFO$_{ar}$ has a relatively poor ignition property by means of ignition delay, leading to abrupt energy conversion and high combustion temperatures. Consequently, the engine could not be operated safely at full load, so the maximum engine load for ULS-HFO$_{ar}$ was reduced from 80 kW (100%) to 68 kW (85%). Fuel properties are listed in Supplementary Table S1, further information of the setup and experiments may be found in Jeong et al.[29].

Prior to the experiments, the engine received a major overhaul and exchange of fuel injector nozzles, sleeve and piston skirt among other. Each change of fuel was accompanied by a change of lubrication oil to enhance the detectability of fuel change on the emissions.

For each combination of fuel and engine load, five samples of PM2.5 were collected at a dilution from 25 to 100, achieved by a two-stage dilution system (eDilutor, Dekati Ltd., Finland), on quartz fiber filters (QFF) for offline analysis. The dilution decreases the exhaust gas temperature and let gas-particle partitioning approach ambient equilibrium. Although different dilution ratios affect the condensation of semi-volatile compounds, the net effect is considered to be small because of generally low contribution of OC1 to TC (Supplementary Table S2). Due to low sampling times of 20 min, revolatilization of sampled PM2.5 ("filter blow-off") is negligible. Conversion to emission factors (EF) was based on exhaust gas flow and engine power as described in Mueller et al.[22].

Multi-wavelength Thermal-optical Carbon Analysis (MW-TOCA)

A punch of 0.5 cm^2 from the QFF was analyzed by a thermo-optical carbon analyzer (DRI TOCA 2001A; Reno, NV, USA) using the temperature protocol *ImproveA*, defining five fractions of organic (OC1-OC4 and OCpyro) and three fractions of elemental carbon (EC1-EC3)[54]. Precisions of the carbon analysis is sample-dependent and range between 2 and 6% for TC and 5 to 10% of the split between OC and EC, according to the manufacturer's manual, but may be larger for high content of OC[37,38]. Laser transmittance (LT) at 635 nm was used to correct apparent EC by pyrolytic OC formed by charring. Furthermore, the TOCA was retrofitted with seven light emitting diodes at 405, 450, 532, 780, 808 and 980 nm[23]. The multi-wavelength TOCA (MW-TOCA) was used to measure the light attenuation (ATN) at individual wavelengths λ, which was obtained from ratio of LT of the untreated filter sample and LT at the end of the TOCA. LT measurement artifacts were corrected considering multiple scattering and shadowing effect by factors R(ATN) including f = 1.1 and C of 2.14[55]. In order to compare the absorptivity of PM2.5 from different marine fuels and loads, the mass absorption efficiency (MAE$_\lambda$) was calculated for the quantified total carbon (TC = OC + EC) by relating ATN at seven wavelengths to the TC filter load [TC], assuming no non-carbonaceous particle components do significantly absorb light:

$$MAE_{TC,\lambda} = \frac{ATN}{R(ATN)\cdot C\cdot[TC]} \quad (3)$$

The uncertainty of the MAE$_{TC,\lambda}$ varies with filter load, wavelength and composition of TC. Median uncertainties for MAE$_\lambda$ in the visible UV and near-infrared range are 25 and 50%, respectively, at 95% confidence.

The spectral MAE(λ) dependence on the wavelength follows a power law

$$MAE(\lambda) = \beta\cdot\lambda^{-\alpha} \quad (4)$$

where α is also called Angström Absorption Exponent (AAE) and β denotes a fitting coefficient. For a wavelength pair, e.g. 405 and 808 nm, the uncertainty of the AAE determination is within ±15% at 95% confidence based on the average precision of 8% for the LT measurement[23], while for the exponential fit, 95% of the individual AAE had an uncertainty within ±50%. All data from MW-TOCA represented mean values of five individually collected filter samples.

Single-particle mass spectrometry

Particulate emissions from the marine engine were fed into a cyclone with a cut-off of 10 µm at a temperature of 200 °C and diluted with an eDiluter (Dekati Ltd.; Kangasala, Finland) before entering a single-particle mass spectrometer (SPMS; Photonion GmbH, Schwerin, Germany). In order to mitigate different concentrations of PM10 in the emissions, dilutions were set to 25 (MGO), 100 (LS-HFO) and 50 (ULS-HFO$_{ar}$).

From a total flow of 1 L min^{-1}, 0.1 L min^{-1} entered the SPMS. Common SPMS system have a steep drop in optical particle detection efficiency below 200 nm. Therefore, to enable the detection range to ultrafine particles (PM0.1), the ionization laser (KrF excimer laser at 248 nm wavelength, pulse energy of 6mJ; PhotonEX, Photonion GmbH, Schwerin, Germany) was operated unsynchronized to optical particle detection at 100 Hz repetition rate[43]. In this so-called free-running mode, particles were randomly hit for laser desorption/ionization (LDI)[51] by the cost of missing particle size information. The spectra were recorded using a 14-bit digitizer (ADQ14, Teledyne SP Devices AB, Sweden) and a customized Labview software., In this study, only carbon clusters (C$_n$ with $n = 2\ldots9$) from negative LDI were considered.

Statistical data analysis

If not otherwise stated, ranges of uncertainty refers to single standard deviations.

The clustering of SPMS data were conducted by adaptive resonance theory neural network algorithm, ART-2a[56]. The program code was taken from the open-source toolkit FATES[57] and embedded in custom MATLAB software (MathWorks Inc.). Carbon cluster related m/z of LDI mass spectra in negative mode were L_2-normalized and clustered using a vigilance factor of 0.8, a learning rate of 0.05, and 20 iterations, followed by a regrouping algorithm to form mean clusters[58].

Data availability

The datasets used and/or analyzed during the current study is partially included the supplementary information and available from the corresponding author on reasonable request.

Received: 9 July 2024; Accepted: 11 November 2024;
Published online: 22 November 2024

References

1. Jalkanen, J.-P., Johansson, L. & Kukkonen, J. A comprehensive inventory of ship traffic exhaust emissions in the European sea areas in 2011. *Atmos. Chem. Phys.* **16**, 71–84 (2016).

2. Corbett, J. J. et al. Mortality from Ship Emissions. A Global Assessment. *Environ. Sci. Technol.* **41**, 8512–8518 (2007).
3. Ershov, M. A. et al. Technological Potential Analysis and Vacant Technology Forecasting in Properties and Composition of Low-Sulfur Marine Fuel Oil (VLSFO and ULSFO) Bunkered in Key World Ports. *J. Mar. Sci. Eng*. **10**, 1828 (2022).
4. Corbin, J. C. et al. Trace Metals in Soot and PM2.5 from Heavy-Fuel-Oil Combustion in a Marine Engine. *Environ. Sci. Technol.* **52**, 6714–6722 (2018).
5. Moldanová, J. et al. Physical and chemical characterisation of PM emissions from two ships operating in European Emission Control Areas. *Atmos. Meas. Tech.* **6**, 3577–3596 (2013).
6. Huang, C. et al. Emission factors of particulate and gaseous compounds from a large cargo vessel operated under real-world conditions. *Environ. Pollut.* **242**, 667–674 (2018).
7. Aakko-Saksa, P. T. et al. Reduction in greenhouse gas and other emissions from ship engines: Current trends and future options. *Prog. Energy Combust. Sci.* **94**, 101055, https://doi.org/10.1016/j.pecs.2022.101055 (2023).
8. The Marine Environment Protection Committee (MEPC). Resolution mepc.192 (61). 2010 guidelines for monitoring the worldwide average sulphur content of fuel oils supplied for use on board ships (2010).
9. The Marine Environment Protection Committee (MEPC). Resolution mepc.329(76). Amendments to the annex of the international convention for the prevention of pollution from ships, 1973, as modified by the protocol of 1978 relating thereto (2021).
10. Chu Van, T., Ramirez, J., Rainey, T., Ristovski, Z. & Brown, R. J. Global impacts of recent IMO regulations on marine fuel oil refining processes and ship emissions. *Transp. Res. D.* **70**, 123–134 (2019).
11. Jeong, S. et al. Aerosol emissions from a marine diesel engine running on different fuels and effects of exhaust gas cleaning measures. *Environ. Pollut.* **316**, 120526 (2023).
12. Lehtoranta, K. et al. Particulate Mass and Nonvolatile Particle Number Emissions from Marine Engines Using Low-Sulfur Fuels, Natural Gas, or Scrubbers. *Environ. Sci. Technol.* **53**, 3315–3322 (2019).
13. Jang, E., Choi, S., Yoo, E., Hyun, S. & An, J. Impact of shipping emissions regulation on urban aerosol composition changes revealed by receptor and numerical modelling. *NPJ Clim. Atmos. Sci.* **6**, 52 (2023).
14. Repka, S. et al. Assessing the costs and environmental benefits of IMO regulations of ship-originated SOx and NOx emissions in the Baltic Sea. *Ambio* **50**, 1718–1730 (2021).
15. van Roy, W. et al. International maritime regulation decreases sulfur dioxide but increases nitrogen oxide emissions in the North and Baltic Sea. *Commun. Earth Environ*. **4**, https://doi.org/10.1038/s43247-023-01050-7 (2023).
16. Wu, D. et al. Primary Particulate Matter Emitted from Heavy Fuel and Diesel Oil Combustion in a Typical Container Ship: Characteristics and Toxicity. *Environ. Sci. Technol.* **52**, 12943–12951 (2018).
17. Oeder, S. et al. Particulate matter from both heavy fuel oil and diesel fuel shipping emissions show strong biological effects on human lung cells at realistic and comparable in vitro exposure conditions. *PLOS ONE* **10**, e0126536 (2015).
18. Corbin, J. C. et al. Brown and Black Carbon Emitted by a Marine Engine Operated on Heavy Fuel Oil and Distillate Fuels: Optical Properties, Size Distributions, and Emission Factors. *J. Geophys. Res. Atmos.* **123**, 6175–6195 (2018).
19. Corbin, J. C. et al. Infrared-absorbing carbonaceous tar can dominate light absorption by marine-engine exhaust. *NPJ Clim. Atmos. Sci.* **2**, 3985–3994 (2019).
20. Santos, L. F. E. D. et al. Marine Fuel Regulations and Engine Emissions: Impacts on Physicochemical Properties, Cloud Activity and Emission Factors. *J. Geophys. Res. Atmos*. **129**, https://doi.org/10.1029/2023JD040389 (2024).
21. Sofiev, M. et al. Cleaner fuels for ships provide public health benefits with climate tradeoffs. *Nat. Commun.* **9**, 406 (2018).
22. Mueller, L. et al. Characteristics and temporal evolution of particulate emissions from a ship diesel engine. *Appl. Energy* **155**, 204–217 (2015).
23. Chen, L.-W. A. et al. Multi-wavelength optical measurement to enhance thermal/optical analysis for carbonaceous aerosol. *Atmos. Meas. Techn.* **8**, 451–461 (2015).
24. Passig, J. et al. Detection of ship plumes from residual fuel operation in emission control areas using single-particle mass spectrometry. *Atmos. Meas. Tech.* **14**, 4171–4185 (2021).
25. Anders, L. et al. Polycyclic aromatic hydrocarbons as fuel-dependent markers in ship engine emissions using single-particle mass spectrometry. *Environ. Sci. Atmos*. https://doi.org/10.1039/D4EA00035H (2024).
26. Zhang, F. et al. Emission factors for gaseous and particulate pollutants from offshore diesel engine vessels in China. *Atmos. Chem. Phys.* **16**, 6319–6334 (2016).
27. Hou, W. et al. On-board measurements of OC/EC ratio, mixing state, and light absorption of ship-emitted particles. *Sci. Tot. Environ.* **904**, 166692 (2023).
28. Lähteenmäki-Uutela, A., Yliskylä-Peuralahti, J., Repka, S. & Mellqvist, J. What explains SECA compliance: rational calculation or moral judgment? *WMU J. Marit. Aff.* **18**, 61–78 (2019).
29. Jeong, S. et al. In vitro genotoxic and mutagenic potentials of combustion particles from marine fuels with different sulfur contents. *bioRxiv,* https://doi.org/10.1101/2024.06.27.601016 (2024).
30. Han, Y. et al. Evaluation of the thermal/optical reflectance method for discrimination between char- and soot-EC. *Chemosphere* **69**, 569–574 (2007).
31. Zhu, J., Lee, K. O., Yozgatligil, A. & Choi, M. Y. Effects of engine operating conditions on morphology, microstructure, and fractal geometry of light-duty diesel engine particulates. *Proc. Combust. Inst.* **30**, 2781–2789 (2005).
32. Elmquist, M., Cornelissen, G., Kukulska, Z. & Gustafsson, Ö. Distinct oxidative stabilities of char versus soot black carbon: Implications for quantification and environmental recalcitrance. *Glob. Biogeochem. Cycl*. **20**, https://doi.org/10.1029/2005GB002629 (2006).
33. Zhao, B. et al. Impact of sulfur functional groups on physicochemical properties and oxidation reactivity of diesel soot particles. *Fuel* **327**, 125041 (2022).
34. Zhang, Z.-H. & Balasubramanian, R. Effects of Cerium Oxide and Ferrocene Nanoparticles Addition As Fuel-Borne Catalysts on Diesel Engine Particulate Emissions: Environmental and Health Implications. *Environ. Sci. Technol.* **51**, 4248–4258 (2017).
35. Streibel, T. et al. Influence of sulphur addition on emissions of polycyclic aromatic hydrocarbons during biomass combustion. *Proc. Combust. Inst.* **35**, 1771–1777 (2015).
36. Khan, M. Y. et al. Benefits of two mitigation strategies for container vessels: cleaner engines and cleaner fuels. *Environ. Sci. Technol.* **46**, 5049–5056 (2012).
37. Aakko-Saksa, P. et al. Considerations in analysing elemental carbon from marine engine exhaust using residual, distillate and biofuels. *J. Aerosol Sci.* **126**, 191–204 (2018).
38. Momenimovahed, A. et al. Comparison of black carbon measurement techniques for marine engine emissions using three marine fuel types. *Aerosol Sci. Technol*. **56**, 46–62 (2022).
39. Zhang, Y., Zhao, K., Lou, D. & Fang, L. Study on the real-world emission characteristics of gaseous and particulate pollutants from an inland ship using a portable emission measurement system. *Mar. Pollut. Bull.* **184**, 114205 (2022).
40. Zhang, F. et al. Size-segregated characteristics of organic carbon (OC), elemental carbon (EC) and organic matter in particulate matter (PM) emitted from different types of ships in China. *Atmos. Chem. Phys.* **20**, 1549–1564 (2020).
41. Chen, Y. & Bond, T. C. Light absorption by organic carbon from wood combustion. *Atmos. Chem. Phys.* **10**, 1773–1787 (2010).

42. Tian, J. et al. Impacts of biomass burning and photochemical processing on the light absorption of brown carbon in the southeastern Tibetan Plateau. *Atmos. Chem. Phys.* **23**, 1879–1892 (2023).
43. Anders, L. et al. Detection of ship emissions from distillate fuel operation via single-particle profiling of polycyclic aromatic hydrocarbons. *Environ. Sci.: Atmos.* **3**, 1134–1144 (2023).
44. Passig, J. et al. Single-particle characterization of polycyclic aromatic hydrocarbons in background air in northern Europe. *Atmos. Chem. Phys.* **22**, 1495–1514 (2022).
45. Jiang, L., Kronbak, J. & Christensen, L. P. The costs and benefits of sulphur reduction measures. Sulphur scrubbers versus marine gas oil. *Transp. Res. D.* **28**, 19–27 (2014).
46. Schneider, E. et al. Humic-like Substances (HULIS) in Ship Engine Emissions: Molecular Composition Effected by Fuel Type, Engine Mode, and Wet Scrubber Usage. *Environ. Sci. Technol.* **57**, 13948–13958 (2023).
47. Sippula, O. et al. Particle emissions from a marine engine: chemical composition and aromatic emission profiles under various operating conditions. *Environ. Sci. Technol.* **48**, 11721–11729 (2014).
48. Diamond, M. S. Detection of large-scale cloud microphysical changes within a major shipping corridor after implementation of the International Maritime Organization 2020 fuel sulfur regulations. *Atmos. Chem. Phys.* **23**, 8259–8269 (2023).
49. Yuan, T. et al. Abrupt reduction in shipping emission as an inadvertent geoengineering termination shock produces substantial radiative warming. *Commun. Earth Environ.* **5**, 281 (2024).
50. Ault, A. P. et al. Characterization of the single particle mixing state of individual ship plume events measured at the Port of Los Angeles. *Environ. Sci. Technol.* **44**, 1954–1961 (2010).
51. Zimmermann, R. & Hanley, L. Photoionization and Photo-Induced Processes in Mass Spectrometry. In *Fundamentals and Applications* (Wiley-VCH, 2021).
52. Passig, J. et al. Resonance-enhanced detection of metals in aerosols using single-particle mass spectrometry. *Atmos. Chem. Phys.* **20**, 7139–7152 (2020).
53. Kobayashi, Y., Furuhata, T., Amagai, K. & Arai, M. Soot precursor measurements in benzene and hexane diffusion flames. *Combust. Flame* **154**, 346–355 (2008).
54. Chow, J. C. et al. The IMPROVE_A Temperature Protocol for Thermal/Optical Carbon Analysis. Maintaining Consistency with a Long-Term Database. *J. Air Waste Manag. Assoc.* **57**, 1014–1023 (2007).
55. Weingartner, E. et al. Absorption of light by soot particles. Determination of the absorption coefficient by means of aethalometers. *J. Aerosol Sci.* **34**, 1445–1463 (2003).
56. Carpenter, G., Grossberg, S. & Rosen, D. B. ART 2-A. An Adaptive Resonance Algorithm for Rapid Category Learning and Recognition. *Neural Netw.* **4**, 493–504 (1991).
57. Sultana, C. M., Cornwell, G. C., Rodriguez, P. & Prather, K. A. FATES. A flexible analysis toolkit for the exploration of single-particle mass spectrometer data. *Atmos. Meas. Tech.* **10**, 1323–1334 (2017).
58. Zhao, W., Hopke, P. K. & Prather, K. A. Comparison of two cluster analysis methods using single particle mass spectra. *Atmos. Environ.* **42**, 881–892 (2008).

Acknowledgements

This study was funded by the Federal Ministry for Economic Affairs and Climate Action (project “SAARUS”, grant number 03SX483D), dtec.bw-Digitalization and Technology Research Center of the Bundeswehr (funded by the European Union – NextGenerationEU, projects “LUKAS” and “MORE”), and the German Science Foundation (Project "PlumeBaSe" ZI 764/32-1; SFB 1477 “Light-Matter Interactions at Interfaces” 441234705). Hendryk Czech ackowledges funding from the Helmholtz Association (Helmholtz International Laboratory aeroHEALTH, grant number InterLabs-0005). We would like to acknowledge Seongho Jeong, Mohammad Saraji-Bozorgzad, Martin Sklorz, and the staff at LKV for their support in the construction of the experimental setup and sample collection.

Author contributions

M.B. conducted the thermal-optical carbon analysis, data processing and evaluation, interpretation of the results and contributed to the manuscript draft. H.C. conceived the study, interpreted the results, performed the statistical data analysis and wrote the manuscript draft. L.A. and J.P. operated the SPMS, conducted its data processing and evaluation. U.E. supervised the experiments, constructed the experimental setup, collected metadata, operated the engine and monitored its performance. J.B. supervised the experiments, constructed the experimental setup, and collected metadata and filter samples. T.S. conceived the study and supervised the experiments. T.W.A., B.B. and R.Z. acquired funding, conceived the study and provided resources. All authors contributed in editing and approved the manuscript.

Funding

Open Access funding enabled and organized by Projekt DEAL.

Competing interests

The authors declare no competing interests.

Additional information

Supplementary information The online version contains supplementary material available at https://doi.org/10.1038/s41612-024-00838-4.

Correspondence and requests for materials should be addressed to Hendryk Czech.